


Effect of finite spin-orbit splitting on the electron-hole exchange interaction in excitons confined in semiconductor nanocrystals

S. V. Goupalov ^{*}

*Department of Physics, Jackson State University, Jackson, Mississippi 39217, USA
and Ioffe Institute, 194021 St. Petersburg, Russia*

 (Received 26 August 2023; revised 28 November 2023; accepted 29 November 2023; published 13 December 2023)

We derive an effective spin-Hamiltonian accounting for the exciton fine structure in quasi-spherical zinc-blende semiconductor nanocrystals within the $\mathbf{k} \cdot \mathbf{p}$ formalism explicitly taking into account the spin-orbit split-off valence band. It is shown that, for excitons in nanocrystals made of III-V and II-VI semiconductors with fairly small spin-orbit splitting, the scaling of the electron-hole exchange interaction with the nanocrystal size insignificantly differs from the inverse nanocrystal volume law predicted within the model neglecting the spin-orbit split-off band. Numerical calculations are performed for InP nanocrystals.

DOI: [10.1103/PhysRevB.108.235419](https://doi.org/10.1103/PhysRevB.108.235419)

I. INTRODUCTION

Colloidal semiconductor nanocrystals, such as CdSe quantum dots, have been used in many applications including optical imaging in biology and medicine. However, in recent years, their less toxic analogs such as InP-based core/shell quantum dots have emerged [1]. Synthesis of high-quality luminescent InP-based core/shell nanocrystals with emission frequencies covering the entire visible spectrum range have been reported and their potential for applications in optoelectronics has been demonstrated [2,3]. Investigation of their fundamental properties has been launched and several studies of exciton fine structure in InP-based core/shell nanocrystals have been performed [4–7].

The fine structure of exciton levels in CdSe nanocrystals has been understood [8,9] within the $\mathbf{k} \cdot \mathbf{p}$ approximation when the valence-band hole is described in the two-band model neglecting the spin-orbit split-off band [10]. However, in InP the spin-orbit splitting amounts to 108 meV [11], which becomes comparable with the energy of the confined hole for InP core diameters below 80 Å [12]. Recently it has been shown [13] that taking into account the admixture of the spin-orbit split-off band is crucial for calculation of the effective g factor of top hole levels in InP nanocrystals. The dark exciton states resulting from the fine-structure splitting can only be revealed in external magnetic fields mixing bright and dark zero-field states and leading to the brightening of the latter [7,14]. Thus a consistent description of the exciton fine structure in InP nanocrystals within the $\mathbf{k} \cdot \mathbf{p}$ approximation should use the three-band model. For nanocrystals, whose overall symmetry is not lower than the cubic symmetry of the underlying crystal lattice, the exciton fine structure is entirely determined by the electron-hole exchange interaction. In this paper, we will assume a quasispherical shape of the nanocrystals and derive an effective spin-Hamiltonian accounting for

the electron-hole exchange interaction within the three-band model.

II. HOLE STATES IN THE THREE-BAND MODEL

The isotropic three-band model describing valence band structure of III-V semiconductors utilizes the generalized Luttinger Hamiltonian [15–17]

$$\hat{H}(\mathbf{k}) = -\frac{\hbar^2 k^2}{2m_0}(\gamma_1 + 4\gamma) + \frac{3\hbar^2 \gamma}{m_0}(\mathbf{k}\hat{\mathbf{I}})^2 + \frac{\Delta}{3}(\hat{\sigma}\hat{\mathbf{I}}) - \frac{\Delta}{3}, \quad (1)$$

where \hbar is Planck's constant, m_0 is the free electron mass, γ_1 and $\gamma \equiv (2\gamma_2 + 3\gamma_3)/5$ are the Luttinger parameters, \hat{I}_α ($\alpha = x, y, z$) are the matrices of angular momenta $I = 1$, Δ is the spin-orbit splitting, and $\hat{\sigma}_\alpha$ are the Pauli matrices. The bands in a bulk semiconductor resulting from this Hamiltonian are shown in Fig. 1 for the case of InP (the parameters are taken from Ref. [12]). The most intuitive method of constructing states of a particle described by such a Hamiltonian and confined in a spherically symmetric potential was developed by Sercel and Vahala [18] for the two-band model and applied to the three-band model by Richard *et al.* [12]. It has also been demonstrated that the same method proves to be very efficient in describing vibrational Lamb modes of spherical particles [19]. The formalism is based on the fact that the differential operator $\hat{H}(-i\nabla)$ commutes with the operator of the total angular momentum $\hat{\mathbf{F}} = \hat{\mathbf{L}} + \hat{\mathbf{J}}$, where $\hat{\mathbf{L}} = -i\hbar \mathbf{r} \times \nabla$, and \hat{J}_α ($\alpha = x, y, z$) are the matrices of angular momenta which can refer to both $J = 3/2$ and $J = 1/2$. In what follows, however, we will only use the notation \hat{J}_α for $J = 3/2$ and use the Pauli matrices for the case of $J = 1/2$. The orbital angular momentum $\hat{\mathbf{L}}$ does not commute with $\hat{H}(-i\nabla)$. Thus, while the total angular momentum F serves as a good quantum number along with its projection F_z onto the z axis and the parity, several values of L , determined by the

^{*}serguei.goupalov@jsums.edu

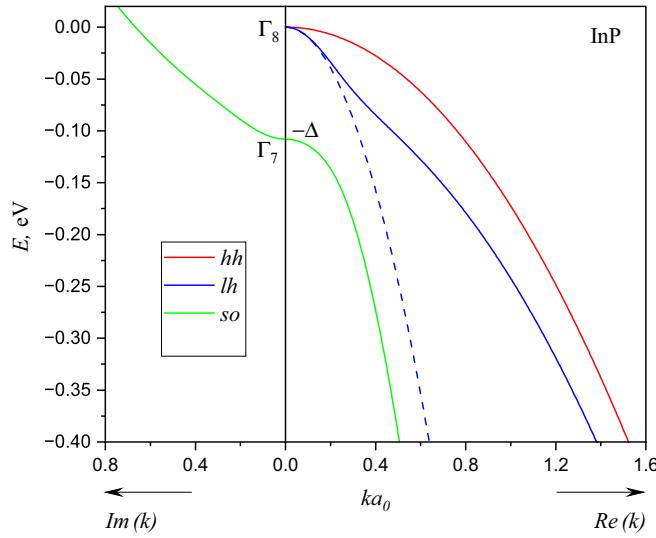


FIG. 1. In the two-band model, levels of size quantization of the valence-band hole originate from the parabolic bands of light (blue dashed line) and heavy (red solid line) holes. In the three-band model, the parabolic band of heavy holes is complemented by nonparabolic bands of the light (blue solid line) and spin-orbit split-off (green solid line) bands. The isotropic energy dispersion is shown in a vicinity of the Γ point of the Brillouin zone as a function of the dimensionless wave number ka_0 , where a_0 is the lattice constant. The Bloch functions at the Γ point transform under the Γ_8 ($J = 3/2$) and Γ_7 ($J = 1/2$) irreducible representations of the point group T_d . Within the two-band (three-band) model, to each energy there correspond two (three) wave numbers from different bands.

$$R_L^{3/2}(r) = C \left[j_L(k_{hh}r) + \frac{(-1)^{L/2} k_{lh}^2 (\rho_{so} + \chi_{so})}{k_{lh}^2 (\rho_{so} + \chi_{so}) + k_{so}^2 (\rho_{lh} - \chi_{lh})} \frac{j_2(k_{hh}a)}{j_2(k_{lh}a)} j_L(k_{lh}r) + \frac{(-1)^{L/2} k_{so}^2 (\rho_{lh} - \chi_{lh})}{k_{lh}^2 (\rho_{so} + \chi_{so}) + k_{so}^2 (\rho_{lh} - \chi_{lh})} \frac{j_2(k_{hh}a)}{j_2(k_{so}a)} j_L(k_{so}r) \right], \quad (4)$$

$$R_2^{1/2}(r) = C \frac{m_0}{\gamma \hbar^2} \frac{(\rho_{lh} - \chi_{lh})(\rho_{so} + \chi_{so})}{k_{lh}^2 (\rho_{so} + \chi_{so}) + k_{so}^2 (\rho_{lh} - \chi_{lh})} j_2(k_{hh}a) \left[\frac{j_2(k_{lh}r)}{j_2(k_{lh}a)} - \frac{j_2(k_{so}r)}{j_2(k_{so}a)} \right]. \quad (5)$$

Here a is the nanocrystal radius, $j_L(x)$ is the spherical Bessel function of the order L and we adapted notations of Ref. [12]:

$$\rho(k) = \frac{1}{2m_0} \sqrt{9\gamma^2 \hbar^4 k^4 - 2\gamma m_0 \Delta \hbar^2 k^2 + m_0^2 \Delta^2},$$

$$\chi(k) = \frac{\Delta}{2} - \frac{\gamma \hbar^2 k^2}{2m_0},$$

$\rho_v \equiv \rho(k_v)$, $\chi_v \equiv \chi(k_v)$, $v = lh, so$. The wave number of the heavy holes is related to the hole energy through

$$k_{hh}^2 = \frac{2m_0|E|}{\hbar^2 (\gamma_1 - 2\gamma)},$$

summation rules for angular momenta, usually contribute to each state of the confined hole. The lowest optically active exciton state is composed of the even hole state with the total angular momentum $F = 3/2$ and the ground electron state. The hole state is contributed by $L = 0, 2$ for $J = 3/2$ and by $L = 2$ for $J = 1/2$. Therefore this state is labeled $1SDD_{3/2}$ [12]. In this paper, we will be concerned with only this hole state. It can be written as

$$|1SDD_{3/2}, F_z\rangle = \sum_{J,\mu} \mathcal{R}_{J,\mu;F_z}(\mathbf{r}) |J, \mu\rangle, \quad (2)$$

where $|J, \mu\rangle$ is the Bloch state at the top of the band Γ_8 when $J = 3/2$ or at the top of the band Γ_7 when $J = 1/2$ (cf. Fig. 1),

$$\mathcal{R}_{J,\mu;F_z}(\mathbf{r}) = \sum_L (-1)^{J-L+F_z} R_L^J(r) \times 2 \sum_M \begin{pmatrix} J & L & \frac{3}{2} \\ \mu & M & -F_z \end{pmatrix} i^L Y_{LM}\left(\frac{\mathbf{r}}{r}\right), \quad (3)$$

$\begin{pmatrix} J & L & \frac{3}{2} \\ \mu & M & -F_z \end{pmatrix}$ is the Wigner $3jm$ symbol which restricts possible values of L and M , $Y_{LM}\left(\frac{\mathbf{r}}{r}\right)$ are the spherical harmonics satisfying $Y_{LM}^*\left(\frac{\mathbf{r}}{r}\right) = (-1)^M Y_{L,-M}\left(\frac{\mathbf{r}}{r}\right)$, and $R_L^J(r)$ are the hole radial wave functions satisfying zero boundary conditions at the nanocrystal surface and defined as follows:

while these of the light and spin-orbit split-off holes satisfy the equation

$$\frac{\hbar^4 k^4}{4m_0^2} (\gamma_1 - 2\gamma)(\gamma_1 + 4\gamma) + \frac{\hbar^2 k^2 (\gamma_1 + 2\gamma)}{2m_0} \Delta - \frac{\hbar^2 k^2 (\gamma_1 + \gamma)}{m_0} |E| + |E|(|E| - \Delta) = 0. \quad (6)$$

One can see from Fig. 1 that, for $E < 0$, k_{lh}^2 is always positive while, from Eq. (6),

$$k_{so}^2 = \frac{|E|(|E| - \Delta) 4m_0^2}{\hbar^4 k_{lh}^2 (\gamma_1 - 2\gamma)(\gamma_1 + 4\gamma)}$$

and becomes negative for $|E| < \Delta$, as seen in Fig. 1. In this case, one should make the following substitutions

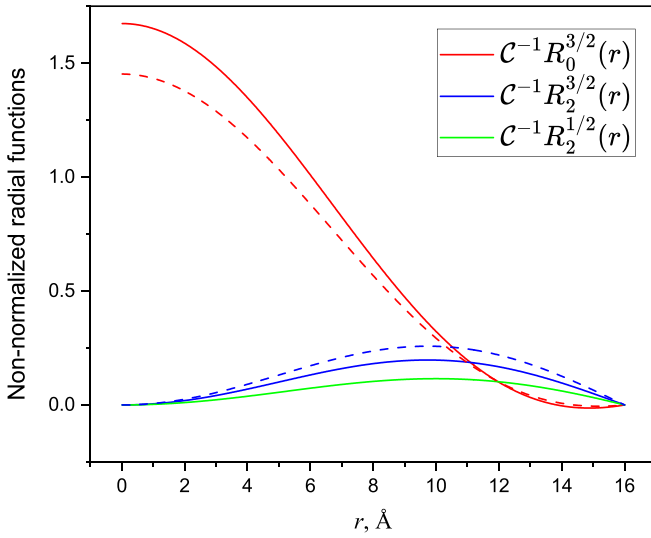


FIG. 2. Non-normalized radial functions $C^{-1}R_L^J(r)$ of the three-band model (solid lines) and their counterparts for the two-band model (dashed lines) for an InP core-only nanocrystal of radius $a = 16 \text{ \AA}$. A spherical hard wall confinement potential is assumed. The functions with $L = 0(2)$ describe radial parts of the s -like (d -like) envelope functions of the $1SDD_{3/2}$ hole state.

in Eqs. (4) and (5): $k_{so} \rightarrow i\kappa_{so}$, $j_L(k_{so}r) \rightarrow i^L i_L^{(1)}(\kappa_{so}r)$, $j_L(k_{so}a) \rightarrow i^L i_L^{(1)}(\kappa_{so}a)$, where $i_L^{(1)}(x)$ is the modified spherical Bessel function.

The energy of the confined hole state is determined from the dispersion equation [12]

$$\begin{aligned} & j_0(k_{hh}a)j_2(k_{lh}a)j_2(k_{so}a)[k_{lh}^2(\rho_{so} + \chi_{so}) + k_{so}^2(\rho_{lh} - \chi_{lh})] \\ & + j_2(k_{hh}a)[k_{lh}^2(\rho_{so} + \chi_{so})j_0(k_{lh}a)j_2(k_{so}a) \\ & + k_{so}^2(\rho_{lh} - \chi_{lh})j_0(k_{so}a)j_2(k_{lh}a)] = 0 \end{aligned} \quad (7)$$

for $|E| > \Delta$ and

$$\begin{aligned} & j_0(k_{hh}a)j_2(k_{lh}a)i_2^{(1)}(\kappa_{so}a)[k_{lh}^2(\rho_{so} + \chi_{so}) - \kappa_{so}^2(\rho_{lh} - \chi_{lh})] \\ & + j_2(k_{hh}a)[k_{lh}^2(\rho_{so} + \chi_{so})j_0(k_{lh}a)i_2^{(1)}(\kappa_{so}a) \\ & + \kappa_{so}^2(\rho_{lh} - \chi_{lh})i_0^{(1)}(\kappa_{so}a)j_2(k_{lh}a)] = 0 \end{aligned} \quad (8)$$

for $|E| < \Delta$. The normalization constant C in Eqs. (4) and (5) is found from the condition

$$\sum_{J,L} \int_0^a dr r^2 [R_L^J(r)]^2 = 1.$$

Non-normalized radial functions, $C^{-1}R_L^J(r)$, are shown in Fig. 2 for an InP nanocrystal of radius $a = 16 \text{ \AA}$, close to the size of the InP core of nanocrystals featured in the single-dot experiments of Refs. [6,7].

The results of the two-band model can be regained in the limit $\Delta \rightarrow \infty$. In particular, in this limit, $\rho_{so} + \chi_{so} \sim \Delta$, $\rho_{lh} - \chi_{lh} \sim 2\gamma^2 \hbar^4 k_{lh}^4 / \Delta m_0^2$. Therefore Eq. (7) yields [10,18]

$$j_0(k_{hh}a)j_2(k_{lh}a) + j_2(k_{hh}a)j_0(k_{lh}a) = 0,$$

while from Eq. (4), we obtain [10]

$$R_L^{3/2}(r) \rightarrow C \left[j_L(k_{hh}r) + (-1)^{L/2} \frac{j_2(k_{hh}a)}{j_2(k_{lh}a)} j_L(k_{lh}r) \right].$$

As emphasized in Refs. [9,10], in the two-band model, $R_L^{3/2}(r) = a^{-3/2} f_L(r/a)$, where $f_L(x)$ is the function introduced in Ref. [9] and depending on the ratio r/a . For this reason, in the two-band model the electron-hole exchange interaction in nanocrystals, where exciton is in the strong confinement regime, scales with the nanocrystal size as a^{-3} [8,9,20]. In the three-band model, one can expect a departure from this dependence.

Since, in the two-band model, for the hole state under consideration, $F = J = 3/2$, the 4×4 matrix (3) becomes a spherical invariant [8,9]. In the three-band model, the matrix (3) has dimension 6×4 .

The lowest conduction band in III-V semiconductors is the twofold spin-degenerate band Γ_6 . The lowest-energy state of the confined electron in this band can be written as

$$|1S_e, m\rangle = \psi_e(\mathbf{r}) |m\rangle,$$

where $\psi_e(\mathbf{r}) = a^{-3/2} \phi(r/a)$ is the electron envelope function which, for the ground state, depends only on the radial coordinate, m is the electron spin index, and $|m\rangle$ is the Bloch function at the bottom of the band Γ_6 .

III. LONG-RANGE ELECTRON-HOLE EXCHANGE INTERACTION

In the effective mass approximation, the matrix element of the electron-hole long-range exchange interaction can be written as [21,22]

$$\begin{aligned} \mathcal{H}_{m'n',mn}^{(\text{long})}(\mathbf{r}'_e, \mathbf{r}'_h, \mathbf{r}_e, \mathbf{r}_h) &= \delta(\mathbf{r}_e - \mathbf{r}_h) \delta(\mathbf{r}'_e - \mathbf{r}'_h) \\ &\times U_{m'n',mn}(\mathbf{r}_e - \mathbf{r}'_e), \end{aligned} \quad (9)$$

where

$$U_{m'n',mn}(\mathbf{r} - \mathbf{r}') = -\frac{\hbar^2 e^2}{m_0^2 E_g^2} \sum_{\alpha\beta} P_{m'n'}^\alpha P_{m\bar{n}}^{\beta*} \frac{\partial^2}{\partial r_\alpha \partial r_\beta} \frac{1}{\varepsilon_1 |\mathbf{r} - \mathbf{r}'|}, \quad (10)$$

E_g is the band gap (for InP, $E_g \gg \Delta$), e is the electron charge, ε_1 is the background dielectric permittivity on the frequency of the excitonic resonance, m and m' are the electron spin indices, $n \equiv J, \mu$ and $n' \equiv J', \mu'$ are the composite hole indices, so that Eqs. (9) and (10) represent 12×12 matrices; $\mathbf{p}_{m\bar{n}} \equiv \langle m | \hat{\mathbf{p}} | \bar{n} \rangle$ is the matrix element of the momentum operator calculated between the electron Bloch states $|m\rangle$ and $|\bar{n}\rangle$ at the band extrema (the hole state $|n\rangle$ and the electron state $|\bar{n}\rangle$ are related via the time-inversion operation).

A correction to the energy of the $1S_e \times 1SDD_{3/2}$ exciton state due to the long-range electron-hole exchange interaction is found in the first order of the perturbation theory:

$$\begin{aligned} H_{m'F'_z, mF_z}^{(\text{long})} &= \sum_{n,n'} \int d\mathbf{r}'_e \int d\mathbf{r}'_h \int d\mathbf{r}_e \int d\mathbf{r}_h \psi_e^*(\mathbf{r}'_e) \\ &\times \mathcal{R}_{F'_z, n'}^\dagger(\mathbf{r}'_h) \mathcal{H}_{m'n', mn}^{(\text{long})}(\mathbf{r}'_e, \mathbf{r}'_h, \mathbf{r}_e, \mathbf{r}_h) \\ &\times \mathcal{R}_{n, F_z}(\mathbf{r}_h) \psi_e(\mathbf{r}_e). \end{aligned} \quad (11)$$

Introducing

$$C_{n, F_z}(\mathbf{r}) = \psi_e(\mathbf{r}) \mathcal{R}_{n, F_z}(\mathbf{r})$$

and substituting Eq. (9) into Eq. (11), we obtain

$$H_{m'F'_z, mF_z}^{(\text{long})} = \sum_{n, n'} \int d\mathbf{r}' \int d\mathbf{r} \times C_{F'_z, n'}^\dagger(\mathbf{r}') U_{m'n', mn}(\mathbf{r} - \mathbf{r}') C_{n, F_z}(\mathbf{r}).$$

As $U_{m'n', mn}(\mathbf{r}, \mathbf{r}') = U_{m'n', mn}(\mathbf{r} - \mathbf{r}')$, it is natural to apply the Fourier transform. An additional simplification comes from the fact that the angular dependence of the Fourier transform of $C_{n, F_z}(\mathbf{r})$ is identical to that of its original. We, therefore, obtain

$$H_{m'F'_z, mF_z}^{(\text{long})} = V^{-1} \sum_{\mathbf{k}} \sum_{n, n'} C_{F'_z, n'}^\dagger(\mathbf{k}) U_{m'n', mn}(\mathbf{k}) C_{n, F_z}(\mathbf{k}), \quad (12)$$

where V is the normalization volume,

$$C_{n, F_z}(\mathbf{k}) = \int d\mathbf{r} C_{n, F_z}(\mathbf{r}) e^{-i\mathbf{k}\mathbf{r}}, \quad (13)$$

$$U_{m'n', mn}(\mathbf{k}) = \frac{4\pi e^2 \hbar^2 (\mathbf{k}\mathbf{p}_{m'\bar{n}})(\mathbf{k}\mathbf{p}_{m\bar{n}})^*}{\varepsilon_1 m_0^2 E_g^2 k^2}. \quad (14)$$

Calculation of the momentum matrix elements in Eq. (14) can be done using explicit form of the Bloch wave functions which may be found in Refs. [16–18]. Otherwise, one can use [9]

$$\langle m|\hat{p}_\sigma|\bar{n}\rangle = \sqrt{2J+1} p_{cv} (-1)^{3/2+J-\sigma} \begin{pmatrix} \frac{1}{2} & J & 1 \\ m & \mu & -\sigma \end{pmatrix}, \quad (15)$$

where \hat{p}_σ is the covariant cyclic component of the momentum operator and $p_{cv} = -i\langle S|\hat{p}_x|X\rangle$ is the interband momentum matrix element. Performing angular integrations and summations in Eq. (12), one obtains

$$\hat{H}^{(\text{long})} = -\eta^{(\text{long})} \left[(\hat{\boldsymbol{\sigma}}\hat{\mathbf{J}}) - \frac{3}{2} \right], \quad (16)$$

where

$$\eta^{(\text{long})} = \frac{\pi a_B^3}{9} \zeta \hbar \omega_{LT}, \quad (17)$$

$$\zeta = \frac{1}{(2\pi)^3} \int_0^\infty dk k^2 [I_0^{3/2}(k) + I_2^{3/2}(k) + I_2^{1/2}(k)]^2, \quad (18)$$

$$I_L^J(k) = 4\pi (-1)^{L/2} \int_0^a dr r^2 \psi_e(r) R_L^J(r) j_L(kr), \quad (19)$$

$$\hbar\omega_{LT} = \frac{4}{\varepsilon_1 a_B^3} \left(\frac{e\hbar p_{cv}}{m_0 E_g} \right)^2$$

is the longitudinal-transverse splitting of the bulk exciton polariton [23,24], a_B is the bulk exciton Bohr radius. We note that the integral in Eq. (19) originates from the radial integral in Eq. (13).

Since the long-range electron-hole exchange interaction is equivalent to the interaction of the bright exciton with the longitudinal electric field induced by its polarization [25], this interaction must vanish for the dark excitonic states. This is guaranteed by the presence of the second term in the square brackets in Eq. (16). However, this constant term only leads to

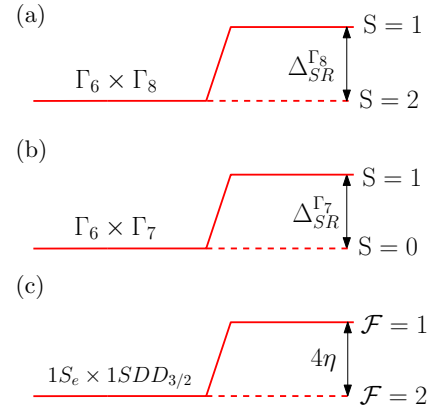


FIG. 3. The short-range electron-hole exchange interaction splits bulk excitons $\Gamma_6 \times \Gamma_8$ (a) and $\Gamma_6 \times \Gamma_7$ (b) into bright and dark excitons characterized by the exciton spin S . In case of the exciton $1S_e \times 1SDD_{3/2}$, confined in a spherical nanocrystal, (c) the bright and dark exciton states are characterized by the values of the total exciton angular momentum $\mathcal{F} = 1$ and $\mathcal{F} = 2$, respectively, while the splitting between them is contributed by both the long-range and the short-range parts of the electron-hole exchange interaction.

the shift of the excitonic level and does not affect its splitting. For this reason, this constant term is usually omitted [8,9].

The two main differences of the three-band model result compared to that of the two-band model [8,9] are appearance of the last term in the square brackets in Eq. (18) and the complex dependence of the functions $R_L^J(r)$ entering Eq. (19) on the nanocrystal size.

In a nanocrystal, the long-range electron-hole exchange correction to the exciton energy has an additional contribution due to the difference in the dielectric constants of the nanocrystal and its environment [9]. As shown in Ref. [9], it is determined only by the s -part of the hole wave function. For this reason, the function $R_2^{1/2}(r)$ does not affect this correction which turns out to be very similar to that of the two-band model. Since, for the two-band model, its detailed derivation was given in Ref. [9], here we will only present the result:

$$\Delta\eta^{(\text{long})} = \frac{2\pi \hbar\omega_{LT}}{3} \left(\frac{a_B}{a} \right)^3 \frac{\varepsilon_1 - \varepsilon_2}{\varepsilon_1 + 2\varepsilon_2} \times \left[\int_0^a dr r^2 \psi_e(r) R_0^{3/2}(r) \right]^2, \quad (20)$$

where ε_2 is the dielectric constant of the nanocrystal's environment.

IV. SHORT-RANGE ELECTRON-HOLE EXCHANGE INTERACTION

The operators of the short-range electron-hole exchange interaction in the bulk semiconductor of the crystal class T_d should be written separately for the $\Gamma_6 \times \Gamma_8$ and $\Gamma_6 \times \Gamma_7$

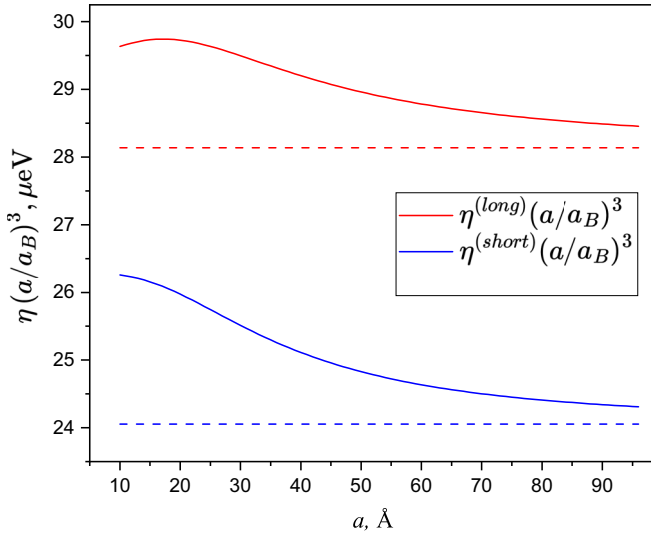


FIG. 4. Size dependencies of the values $\eta^{(\text{long})}(a/a_B)^3$ (red solid line) and $\eta^{(\text{short})}(a/a_B)^3$ (blue solid line) compared to their counterparts calculated within the two-band model (dashed lines) for InP core-only nanocrystals.

excitons (while their Bohr radii are approximately the same):

$$\mathcal{H}_{\Gamma_8}^{(\text{short})}(\mathbf{r}'_e, \mathbf{r}'_h, \mathbf{r}_e, \mathbf{r}_h) = -\frac{\Delta_{SR}^{\Gamma_8} \pi a_B^3}{4} \delta(\mathbf{r}_e - \mathbf{r}'_e) \times \delta(\mathbf{r}_h - \mathbf{r}'_h) \delta(\mathbf{r}_e - \mathbf{r}_h) (\hat{\sigma}_e \hat{\mathbf{J}}), \quad (21)$$

$$\mathcal{H}_{\Gamma_7}^{(\text{short})}(\mathbf{r}'_e, \mathbf{r}'_h, \mathbf{r}_e, \mathbf{r}_h) = \frac{\Delta_{SR}^{\Gamma_7} \pi a_B^3}{4} \delta(\mathbf{r}_e - \mathbf{r}'_e) \times \delta(\mathbf{r}_h - \mathbf{r}'_h) \delta(\mathbf{r}_e - \mathbf{r}_h) (\hat{\sigma}_e \hat{\sigma}_h), \quad (22)$$

where $\Delta_{SR}^{\Gamma_8}$ and $\Delta_{SR}^{\Gamma_7}$ are the splittings between the exciton bright and dark states in a bulk semiconductor (in the isotropic model), see Fig. 3, and we distinguished between the Pauli matrices referring to the electron and hole spin degrees of freedom by the corresponding subscripts. The form of Eqs. (21) and (22) is dictated by the symmetry. The last delta-function in the right-hand sides of Eqs. (21) and (22) reflects the short-range character of the interaction. The two extra delta functions are needed to make Eqs. (21) and (22) compatible with Eq. (11), i.e., to employ the same formalism [21,22] which was used for Eqs. (9), (10). The constants in the right-hand sides of Eqs. (21) and (22) are chosen to match the resulting splittings for the excitons in the bulk. Eqs. (21) and (22) represent 8×8 and 4×4 matrices, respectively. They can be combined to form a 12×12 block-diagonal matrix which may be inserted into an analog of Eq. (11). This will yield

$$\hat{H}^{(\text{short})} = -\eta^{(\text{short})}(\hat{\sigma} \hat{\mathbf{J}}), \quad (23)$$

where

$$\eta^{(\text{short})} = \frac{\Delta_{SR}^{\Gamma_7} \pi a_B^3}{10} \int_0^a dr r^2 \psi_e^2(r) [R_2^{1/2}(r)]^2 + \frac{\Delta_{SR}^{\Gamma_8} \pi a_B^3}{4} \times \int_0^a dr r^2 \psi_e^2(r) \left([R_0^{3/2}(r)]^2 + \frac{1}{5} [R_2^{3/2}(r)]^2 \right). \quad (24)$$

The two main differences of the three-band model result compared to that of the two-band model [8,9,20] are appearance of the first term in the right-hand side of Eq. (24) and the complex dependence of the functions $R_L^J(r)$ entering Eq. (24) on the nanocrystal size.

V. NUMERICAL RESULTS

For numerical calculations, we consider a core-only InP nanocrystal with the electron envelope wave function given by

$$\psi_e(r) = \frac{1}{\sqrt{2\pi a}} \frac{\sin \frac{\pi r}{a}}{r}.$$

The values of $\Delta_{SR}^{\Gamma_8} = 40 \mu\text{eV}$ [23,24] and $\hbar\omega_{LT} = 170 \mu\text{eV}$ [24] are taken from the experiment and the values of $\Delta_{SR}^{\Gamma_7} = 9.26 \mu\text{eV}$ [26] and $a_B = 96 \text{Å}$ [26] were calculated. All the other parameters are taken from Ref. [12]. In Fig. 4, we plot the values of $\eta^{(\text{long})}(a/a_B)^3$ (red solid line) and $\eta^{(\text{short})}(a/a_B)^3$ (blue solid line) calculated according to Eqs. (17) and (24), respectively, as functions of the nanocrystal size and compare them to their counterparts calculated within the two-band model (dashed lines). One can see that both parameters demonstrate very weak size dependence and are very close to the results of the two-band model.

VI. CONCLUSIONS

We have derived an effective spin-Hamiltonian accounting for the exciton fine structure in quasispherical zinc-blende semiconductor nanocrystals within the $\mathbf{k} \cdot \mathbf{p}$ formalism explicitly taking into account the spin-orbit split-off valence band. Although this leads to a difference in the scaling law of the electron-hole exchange interaction with the nanocrystal size from that predicted within the two-band model, the quantitative difference turns out to be small. In other words, even within the three-band model, for excitons, strongly confined in nanocrystals made of III-V and II-VI semiconductors with fairly small spin-orbit splitting, the scaling of electron-hole exchange interaction with nanocrystal size insignificantly differs from the inverse nanocrystal volume law. In the meantime, the three-band model is more general and contains the results of the two-band model in the limit $\Delta \rightarrow \infty$. Therefore analytical expressions for exchange splittings obtained in this work for arbitrary Δ can prove to be useful.

ACKNOWLEDGMENTS

The author wishes to thank Brahim Lounis and Philippe Tamarat for stimulating discussions. This work was supported by the U.S. National Science Foundation through DMR-2100248.

- [1] V. Brunetti, H. Chibli, R. Fiammengo, A. Galeone, M. A. Malvindi, G. Vecchio, R. Cingolani, J. L. Nadeaub, and P. P. Pompa, InP/ZnS as a safer alternative to CdSe/ZnS core/shell quantum dots: in vitro and in vivo toxicity assessment, *Nanoscale* **5**, 307 (2013).
- [2] Y.-H. Won, O. Cho, T. Kim, D.-Y. Chung, T. Kim, H. Chung, H. Jang, J. Lee, D. Kim, and E. Jang, Highly efficient and stable InP/ZnSe/ZnS quantum dot light-emitting diodes, *Nature (London)* **575**, 634 (2019).
- [3] H. Van Avermaet, P. Schiettecatte, S. Hinz, L. Giordano, F. Ferrari, C. Nayral, F. Delpech, J. Maultzsch, H. Lange, and Z. Hens, Full-spectrum Inp-based quantum dots with near-unity photoluminescence quantum efficiency, *ACS Nano* **16**, 9701 (2022).
- [4] L. Biadala, B. Siebers, Y. Beyazit, M. D. Tessier, D. Dupont, Z. Hens, D. R. Yakovlev, and M. Bayer, Band-edge exciton fine structure and recombination dynamics in InP/ZnS colloidal nanocrystals, *ACS Nano* **10**, 3356 (2016).
- [5] A. Brodu, M. V. Ballottin, J. Buhot, E. J. van Harten, D. Dupont, A. La Porta, P. T. Prins, M. Tessier, M. A. M. Versteegh, V. Zwiller, S. Bals, Z. Hens, F. T. Rabouw, P. C. M. Christianen, C. de Mello Donega, and D. Vanmaekelbergh, Exciton fine structure and lattice dynamics in InP/ZnSe core/shell quantum dots, *ACS Photonics* **5**, 3353 (2018).
- [6] A. Brodu, V. Chandrasekaran, L. Scarpelli, J. Buhot, F. Masia, M. V. Ballottin, M. Severijnen, M. D. Tessier, D. Dupont, F. T. Rabouw, P. C. M. Christianen, C. de Mello Donega, D. Vanmaekelbergh, W. Langbein, and Z. Hens, Fine structure of nearly isotropic bright excitons in InP/ZnSe colloidal quantum dots, *J. Phys. Chem. Lett.* **10**, 5468 (2019).
- [7] E. Prin, C. Xia, Y.-H. Won, E. Jang, S. V. Goupalov, P. Tamarat, and B. Lounis, Revealing the band-edge exciton fine structure of single InP nanocrystals, *Nano Lett.* **23**, 6067 (2023).
- [8] S. V. Goupalov and E. L. Ivchenko, Electron-hole long-range exchange interaction in semiconductor quantum dots, *J. Cryst. Growth* **184-185**, 393 (1998).
- [9] S. V. Goupalov and E. L. Ivchenko, The fine structure of excitonic levels in CdSe nanocrystals, *Fiz. Tverd. Tela* **42**, 1976 (2000) [*Phys. Solid State* **42**, 2030 (2000)].
- [10] A. L. Efros, Luminescence polarization of CdSe microcrystals, *Phys. Rev. B* **46**, 7448 (1992).
- [11] J. Camassel, P. Merle, L. Bayo, and H. Mathieu, Deformation potentials of the fundamental exciton spectrum of InP, *Phys. Rev. B* **22**, 2020 (1980).
- [12] T. Richard, P. Lefebvre, H. Mathieu, and J. Allègre, Effects of finite spin-orbit splitting on optical properties of spherical semiconductor quantum dots, *Phys. Rev. B* **53**, 7287 (1996).
- [13] M. A. Semina, A. A. Golovatenko, and A. V. Rodina, Influence of the spin-orbit split-off valence band on the hole g factor in semiconductor nanocrystals, *Phys. Rev. B* **104**, 205423 (2021).
- [14] C. Sinito, M. J. Fernée, S. V. Goupalov, P. Mulvaney, P. Tamarat, and B. Lounis, Tailoring the exciton fine structure of cadmium selenide nanocrystals with shape anisotropy and magnetic field, *ACS Nano* **8**, 11651 (2014).
- [15] M. I. Dyakonov and V. I. Perel, Spin orientation of electrons associated with the interband absorption of light in semiconductors, *Zh. Eksp. Teor. Fiz.* **60**, 1954 (1971) [*Sov. Phys. JETP* **33**, 1053 (1971)].
- [16] V. N. Abakumov, V. I. Perel, and I. N. Yassievich, *Nonradiative Recombination in Semiconductors*, Vol. 33 of Modern Problems in Condensed Matter Sciences, edited by V. M. Agranovich and A. A. Maradudin (Elsevier, New York, 1991).
- [17] M. I. Dyakonov and V. I. Perel, *Theory of optical spin orientation of electrons and nuclei in semiconductors*, in *Optical Orientation*, edited by F. Meier and B. P. Zakharchenya, Vol. 8 of Modern Problems in Condensed Matter Sciences, edited by V. M. Agranovich and A. A. Maradudin (Elsevier, New York, 1984).
- [18] P. C. Sercel and K. J. Vahala, Analytical formalism for determining quantum-wire and quantum-dot band structure in the multiband envelope-function approximation, *Phys. Rev. B* **42**, 3690 (1990).
- [19] S. V. Goupalov, Classical problems in the theory of elasticity and the quantum theory of angular momentum, *Usp. Fiz. Nauk* **190**, 63 (2020) [*Phys.-Usp.* **63**, 57 (2020)].
- [20] A. L. Efros, M. Rosen, M. Kuno, M. Nirmal, D. J. Norris, and M. Bawendi, Band-edge exciton in quantum dots of semiconductors with a degenerate valence band: Dark and bright exciton states, *Phys. Rev. B* **54**, 4843 (1996).
- [21] G. E. Pikus and G. L. Bir, Exchange interaction in excitons in semiconductors, *Zh. Eksp. Teor. Fiz.* **60**, 195 (1971) [*Sov. Phys. JETP* **33**, 108 (1971)].
- [22] G. L. Bir and G. E. Pikus, *Symmetry and Strain-Induced Effects in Semiconductors* (Wiley, New York, 1974).
- [23] W. Ekardt, K. Löscher, and D. Bimberg, Determination of the analytical and the nonanalytical part of the exchange interaction of InP and GaAs from polariton spectra in intermediate magnetic fields, *Phys. Rev. B* **20**, 3303 (1979).
- [24] H. Mathieu, Y. Chen, J. Camassel, J. Allegre, and D. S. Robertson, Excitons and polaritons in InP, *Phys. Rev. B* **32**, 4042 (1985).
- [25] S. V. Goupalov, P. Lavallard, G. Lamouche, and D. S. Citrin, Electrodynamical treatment of the electron-hole long-range exchange interaction in semiconductor nanocrystals, *Fiz. Tverd. Tela* **45**, 730 (2003) [*Phys. Solid State* **45**, 768 (2003)].
- [26] H. Fu, L.-W. Wang, and A. Zunger, Excitonic exchange splitting in bulk semiconductors, *Phys. Rev. B* **59**, 5568 (1999).